Nanofluidic flow assisted assembly of dispersed plasmonic nanostructures into shallow nanochannel sensors

Hongsuk Nam and Jeong Seop YoonHiroto IzuokaBo-Ram Oh and Katsuo KurabayashiWenjie WanXiaogan Liang

Citation: Journal of Vacuum Science & Technology B, Nanotechnology and Microelectronics: Materials, Processing, Measurement, and Phenomena **34**, 06KM04 (2016); doi: 10.1116/1.4967748

View online: http://dx.doi.org/10.1116/1.4967748

View Table of Contents: http://avs.scitation.org/toc/jvb/34/6

Published by the American Vacuum Society

Articles you may be interested in

Study of alternate hardmasks for extreme ultraviolet patterning
Journal of Vacuum Science & Technology B, Nanotechnology and Microelectronics: Materials, Processing, Measurement, and Phenomena **34**, 06KG0306KG03 (2016); 10.1116/1.4966960

Crystallization of nanoscale NiTi alloy thin films using rapid thermal annealing
Journal of Vacuum Science & Technology B, Nanotechnology and Microelectronics: Materials, Processing, Measurement, and Phenomena **34**, 06KK0106KK01 (2016); 10.1116/1.4963375

Bim+ ion beam patterning of germanium surfaces at different temperatures and ion fluence
Journal of Vacuum Science & Technology B, Nanotechnology and Microelectronics: Materials, Processing, Measurement, and Phenomena **34**, 061805061805 (2016); 10.1116/1.4967697

Replication of nanopits and nanopillars by roll-to-roll extrusion coating using a structured cooling roll
Journal of Vacuum Science & Technology B, Nanotechnology and Microelectronics: Materials, Processing, Measurement, and Phenomena **34**, 06KM0206KM02 (2016); 10.1116/1.4967217

High-resolution, high-aspect-ratio iridium–nickel composite nanoimprint molds
Journal of Vacuum Science & Technology B, Nanotechnology and Microelectronics: Materials, Processing, Measurement, and Phenomena **34**, 061804061804 (2016); 10.1116/1.4967696

Aluminum-based contacts for use in GaSb-based diode lasers
Journal of Vacuum Science & Technology B, Nanotechnology and Microelectronics: Materials, Processing, Measurement, and Phenomena **34**, 061207061207 (2016); 10.1116/1.4967300

HIDEN ANALYTICAL
Instruments for Advanced Science

Contact Hiden Analytical for further details:
www.HidenAnalytical.com
info@hiden.co.uk
CLICK TO VIEW our product catalogue

Gas Analysis
dynamic measurement of reaction gas streams
catalysis and thermal analysis
molecular beam studies
dissolved species probes
fermentation, environmental and ecological studies

Surface Science
UHV TPD
SIMS
end point detection in ion beam etch
elemental imaging - surface mapping

Plasma Diagnostics
plasma source characterization
etch and deposition process reaction
kinetic studies
analysis of neutral and radical species

Vacuum Analysis
partial pressure measurement and control of process gases
reactive sputter process control
vacuum diagnostics
vacuum coating process monitoring

CrossMark

Nanofluidic flow assisted assembly of dispersed plasmonic nanostructures into shallow nanochannel sensors

Hongsuk Nam[a] and Jeong Seop Yoon[a]
Department of Mechanical Engineering, University of Michigan, 2350 Hayward Avenue, Ann Arbor, Michigan 48109

Hiroto Izuoka[a]
Department of Mechanical Science and Engineering, Nagoya University, Furo-cho, Chikusa-ku, Nagoya, Aichi 464-8603, Japan

Bo-Ram Oh and Katsuo Kurabayashi
Department of Mechanical Engineering, University of Michigan, 2350 Hayward Avenue, Ann Arbor, Michigan 48109

Wenjie Wan
University of Michigan-Shanghai Jiao Tong University Joint Institute and Department of Physics and Astronomy, Shanghai Jiao Tong University, Shanghai 200240, China

Xiaogan Liang[b]
Department of Mechanical Engineering, University of Michigan, 2350 Hayward Avenue, Ann Arbor, Michigan 48109

(Received 24 June 2016; accepted 31 October 2016; published 9 November 2016)

The authors present a method for assembling plasmonic nanostructures into already-sealed shallow nanochannel-based nanofluidic sensor structures. This method is termed as nanofluidic-flow-assisted-assembly (NFAA). NFAA utilizes nanofluidic flows with large shear rate and stress to deposit high-areal-density, well-dispersed plasmonic nanoparticles (NPs) into shallow nanochannel sensing areas. In particular, in a NFAA process, the nano/microfluidic structures are first patterned into a Si or SiO_2 substrate and permanently sealed with fused quartz coverslips using plasma sealing. Afterward, a colloidal solution of plasmonic NPs is driven into the shallow nanochannel structures. In the shallow nanochannel areas, the large shear rate and stress of the nanofluidic colloidal solution flow results in the deposition of well-dispersed NPs and effectively prevents undesirable aggregation of NPs. Using NFAA, the authors have demonstrated the deposition of well-dispersed Au NPs with various areal densities (10^2–$10^4\,\mu m^{-2}$) into shallow nanochannels. The light absorbance peak of NFAA-coated Au NPs exhibits the narrower full-width-at-half-maximum than that of the Au NPs directly deposited from a colloidal solution, further indicating that NFAA can result in the higher degree of dispersion of high-density NPs. The authors also demonstrated that the additional nanoscale anchoring structures prepatterned in a shallow nanochannel, in combination with NFAA processes, can enable selective deposition of functional nanoparticles around designated locations. This work provides a nanofabrication scheme for introducing functional nanostructures into already-sealed nanofluidic structures. This method could be further generalized to enable integration of various electrically/optically active nanoscale components into permanently sealed nano/microfluidic structures and therefore address the incompatibility among the fabrication routes of these device structures. © *2016 American Vacuum Society*.
[http://dx.doi.org/10.1116/1.4967748]

I. INTRODUCTION

The sensing techniques utilizing plasmonic properties of metallic nanostructures [e.g., nanoparticles (NPs) and nanorods (NRs)] have been a subject of considerable interest lately because of their high detection sensitivity and low limit-of-detection.[1,2] Examples of such plasmonic device principles include localized surface plasmon resonance (LSPR) and surface-enhanced Raman scattering.[3–10] The fabrication of some specific plasmonic sensors, such as the sensors requiring an integration of permanently sealed nano/microfluidic structures and plasmonic nanostructures,[11,12] involves the deposition of high-areal-density, well-dispersed metal nanostructures on solid surfaces as well as the sealing of nano/microfluidic structures through plasma-assisted bonding of coverslips. However, the demands of a high deposition density and a high degree of dispersion of metal nanostructures stand in a trade-off to each other. Especially, high deposition densities result in significant aggregation of nanostructures and undesirable interparticle plasmonic coupling for the aforementioned sensor applications.[11,12] Because of this reason, the regular deposition methods without involving any additional surface functionalization processes (e.g., direct deposition of unfunctionalized nanoparticles from a colloidal solution onto an untreated open surface) usually result in deposition densities

[a]H. Nam, J. S. Yoon, and H. Izuoka contributed equally to this work.
[b]Electronic mail: xiaoganl@umich.edu

lower than ~0.2 NP/μm^2.[13] Grabar *et al*. demonstrated deposition of well-dispersed, high-density nanoparticles on open surfaces without using any confined flows.[14] However, this method needs special surface derivatization processes and relatively long processing times up to 24 h. Furthermore, the aggregation of high-density plasmonic nanostructures also results in a too poor fabrication yield to enable scale-up biosensor arrays for practical multiplexing sensing applications. In addition to the trade-off between the deposition density and the dispersion degree of plasmonic nanostructures, such plasmonic/nanofluidic-integrated sensors as well as other sensor applications involving the integration of electrically/optically active nanoscale components and permanently sealed nano/microfluidic structures suffer from additional challenges associated with the incompatibility among the fabrication routes of these device structures. Specifically, the practical sensor applications need permanently sealed nanofluidic structures made from Si or SiO_2-based inorganic materials.[15,16] The sealing process needs wet cleaning steps based on strong chemicals [e.g., piranha and Radio-Company-of-America (RCA) cleaning approaches] for eliminating particles and contaminants that prevent the bonding of coverslips. In such strong chemicals at elevated temperatures, some electrically/optically active nanoscale components (e.g., metal NPs, sensing transistors, and low-dimensional semiconductor nanostructures) cannot survive. Especially, for a very common plasmonic device system, in which metallic nanostructures are lithographically fabricated on Si or SiO_2 substrates, RCA and piranha processes can seriously reduce the adhesion at the metal/SiO_2 interfaces and result in undesirable strippling of metallic nanostructures (in fact, RCA and piranha processes are commonly used to remove metallic contaminants for fabricating other devices). After such wet cleaning processes, energetic plasma treatment is performed to activate the bonding sites on Si/SiO_2 surfaces for subsequent bonding. Such plasma treatment also results in damages, to some extent, to the active device components.[17] Here, it should be noted that O_2 plasma is sometimes used for cleaning metal nanostructures. However, such O_2 plasma recipes for cleaning purposes have relatively low power densities. To activate the oxide-based surfaces for bonding coverslips, people usually need inductively induced O_2 plasma species that have much higher power densities and can seriously damage most electronic/photonic nanostructures, including metal structures.[15,16,18–20] Therefore, the electrically/optically active components have to be fabricated after the sealing of nano/microfluidic structures. However, after the sealing step, the conventional planar nanofabrication techniques cannot introduce such active components into sealed fluidic spaces. To address these nanofabrication challenges, new generic nanoplasmonics/nanofluidics-compatible nanofabrication methods are demanded.

In this article, we report a nanofabrication method for depositing plasmonic NPs (e.g., Au NPs) into shallow nanochannel-based nanofluidic device structures. This method is termed as nanofluidic flow-assisted assembly (NFAA), in which the NP colloidal flows driven into permanently sealed shallow nanochannel structures can result in the deposition of high-areal-density, well-dispersed NPs free of aggregation. This work also involves the study on the dependence of the resultant areal densities of deposited nanostructures on the shallow nanochannel depths. Using NFAA processes, we have specifically demonstrated the deposition of high-areal-density, well-dispersed Au NPs in Si-based shallow nanochannel sensors. Furthermore, we characterized the light absorbance peaks of the Au NPs deposited by NFAA and direct deposition from a colloidal solution. We found that the full-width-at-half-maximum (FWHM) of the absorbance peak measured from NFAA-coated Au NPs is narrower than that of directly deposited NPs with using same functionalization method. This further indicates that NFAA processes result in the higher degree of dispersion of deposited NPs in comparison with direct deposition processes. Finally, we fabricated a set of addressable anchoring nanostructures in Si-based shallow nanochannel channels. Such anchoring nanostructures in combination with NFAA processes can enable selective deposition of plasmonic NPs around designated locations in permanently sealed nanofluidic device structures.

II. RESULTS AND DISCUSSION

Figure 1(a) schematically illustrates the nanofluidic-flow-assisted assembly (NFAA) process for depositing plasmonic NPs into a shallow nanochannel sensor structure. In such a NFAA process, the shallow nanochannels as well as other functional nano/microfluidic components are first fabricated in a Si or SiO_2 substrate and permanently sealed with a fused quartz coverslip using plasma-assisted bonding.[15,16] After sealing, a colloidal solution containing plasmonic NPs is driven into the shallow nanochannels using a liquid pumping system that can generate a constant pressure drop of ~1 atm across the nanochannels. Driven by such a constant pressure drop, both the average flow rate (Q) and the average NP moving speed (V) in shallow nanochannels decrease with the reduction of the nanochannel depth (d) (i.e., $Q = \Delta P w d^3/12\,\mu L$ and $V = \Delta P d^2/12\,\mu L$, where ΔP is the pressure drop across the nanochannels; μ is the viscosity of the colloidal solution; L is the nanochannel length; w is the nanochannel width). Therefore, with the reduction of the nanochannel depth, the probability for NPs being deposited onto the top and bottom surfaces of shallow nanochannels is expected to prominently increase and result in a higher areal density of deposited NPs given a fixed processing time (or flow time duration). In addition, the Z-direction confinement due to the shallow nanochannel structure is anticipated to effectively suppress the undesirable aggregation of NPs and result in a high degree of dispersion of deposited NPs. Right now, self-assembly methods can indeed produce well-dispersed nanostructures.[21] Currently, we do not expect that the presented NFAA method is advantageous over self-assembly methods in terms of the resulted areal density and degree of dispersion of deposited nanostructures. However, most self-assembly methods for generating well-dispersed nanostructures need special chemical processes and materials for functionalizing surfaces of nanostructures that are to be deposited, whereas the presented NFAA method does not need them. Therefore, NFAA could likely serve as a simple

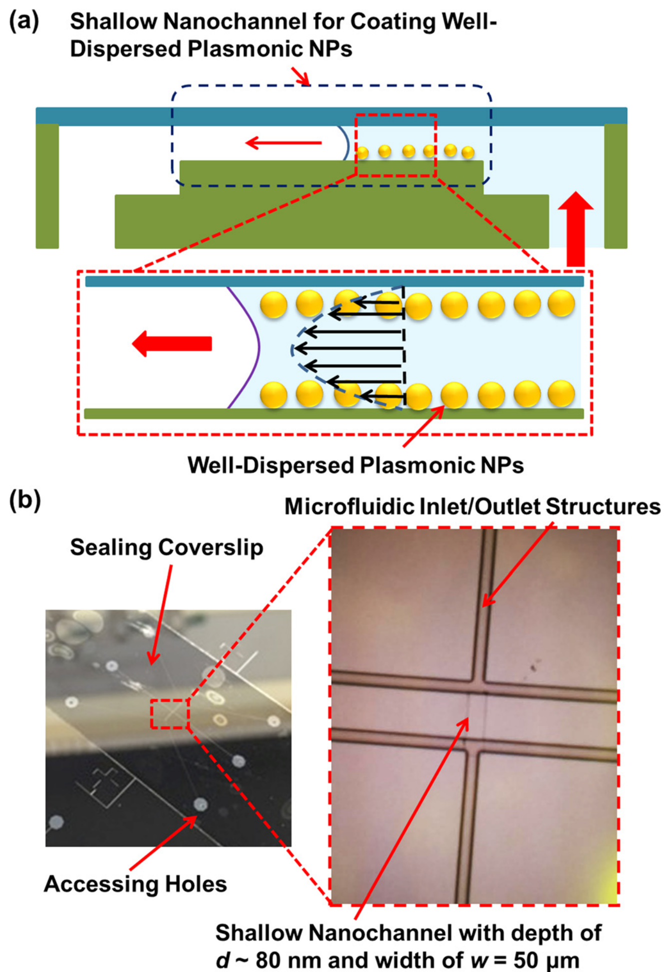

FIG. 1. (Color online) (a) Schematic illustration of a shallow nanochannel sensor structure, in which a nanofluidic colloidal flow with large shear rate results in deposition of high-areal-density, well-dispersed plasmonic NPs; (b) photograph and zoomed optical micrograph of a representative shallow nanochannel sensor, which has been permanently sealed with a fused quartz coverslip. In this work, the shallow nanochannel width is fixed to 50 μm, and the shallow nanochannel depth ranges from 80 to 500 nm.

and cost-effective deposition approach for making plasmonic sensing devices.

In this work, the shallow nanochannels and other nano/microfluidic structures are fabricated by using a standard planar fabrication route. Specifically, the shallow nanochannels (width: 50 μm, length: 500 μm, and depth: 100–800 nm) are fabricated in 0.5 mm thick Si or fused silica substrates using photolithography followed with dry etching in a plasma etcher (LAM 9400 SE, LAM Research Corporation). The standard H-shaped microfluidic inlet/outlet channels (depth: 5–10 μm) are subsequently structured and aligned with the shallow nanochannels by using photolithography followed with deep reactive ion etching (STS Pegasus 4, SPTS Technologies, Ltd.). Afterward, a thick photoresist film ($\sim$100 μm thick) is covered onto the whole device substrate and hardened at 80 °C overnight to protect already fabricated nano/microfluidic structures during the subsequent drilling process for creating the through holes for accessing inlet/outlet microfluidic channels. Using a sandblasting tool with 30 μm size alumina particles, $\sim$1 mm diameter accessing holes are drilled through the device substrate without damaging shallow nanochannels and inlet/outlet channels. After the drilling process, the protective photoresist film is removed using isopropyl alcohol that results in a relatively slow rate for dissolving the photoresist and can effectively avoid the redeposition of alumina particles onto the cleaned device substrate. Before the sealing of nano/microfluidic structures, both the device substrate and the fused silica coverslip (0.13 mm thick) are thoroughly cleaned using the standard RCA process (i.e., deionized (DI) water: NH_4OH: $H_2O_2 = 5$: 1: 1, 75 °C, 15 min) followed with DI water rinse. Finally, the cleaned substrate bearing nano/microfluidic structures and the flat coverslip are bonded together after an O_2 plasma surface treatment (RF power: 500 W, duration: 30 s). Figure 1(b) displays the photograph and optical micrograph of a representative 80 nm deep shallow nanochannel device, which has been permanently sealed with a fused quartz coverslip.

During a NFAA process, we utilize a lab-made liquid jig to connect the outlet holes of a shallow nanochannel device with a vacuum pump, and the inlet holes are open to atmosphere. The colloidal solution containing 5 nm size Au NPs (concentration: 0.05 mg/ml) is filled into the device through the inlet holes and driven into shallow nanochannels by the pressure drop ($\sim$1 atm pressure) between the inlet and outlet holes. For each NFAA process, such nanofluidic flows of the Au NP colloidal solution last for 6 h to obtain a sizable amount of Au NPs deposited in the shallow nanochannel areas.

To evaluate the areal densities and the dispersion degrees of NFAA-deposited Au NPs in shallow nanochannels, we intentionally removed the sealing coverslips and acquired scanning electron micrographs (SEMs) of NFAA-deposited Au NPs in the shallow nanochannels with various depths. Figure 2(a) shows the low-magnification SEM image of a shallow nanochannel device with 100 nm deep shallow nanochannels and 10 μm deep microfluidic inlet/outlet channels. Figure 2(b) displays a zoomed view [corresponding to the region denoted by the dashed box in Fig. 2(a)] of the microfluidic inlet channel, in which a significant aggregation of deposited Au NPs can be observed, and there is almost no region with dispersed NPs. The sizes of observed Au NP agglomerations range from 100 to 500 nm. Figures 2(c) and 2(d) display the zoomed views [corresponding to the region denoted by the red box in Fig. 2(a)] of a shallow nanochannel region, over which the Au NPs are well dispersed with a high areal density of $\sim 10^4$ NP/μm^2. These results show that the application of the shallow nanochannel structure for depositing NPs from a colloidal solution can effectively suppress the undesirable aggregation of NPs and result in well dispersed NPs with a high areal density. This desirable effect is attributed to the low flow rate (or velocity) of the nanofluidic flow in the shallow nanochannel as well as the shallow nanochannel-induced Z-direction confinement of the motion of NPs. The nanoparticles deposited in our shallow nanochannels by using NFAA processes still exhibit some extent of aggregation, and therefore, the interparticle plasmonic coupling is expected to still exist. However, given a similar

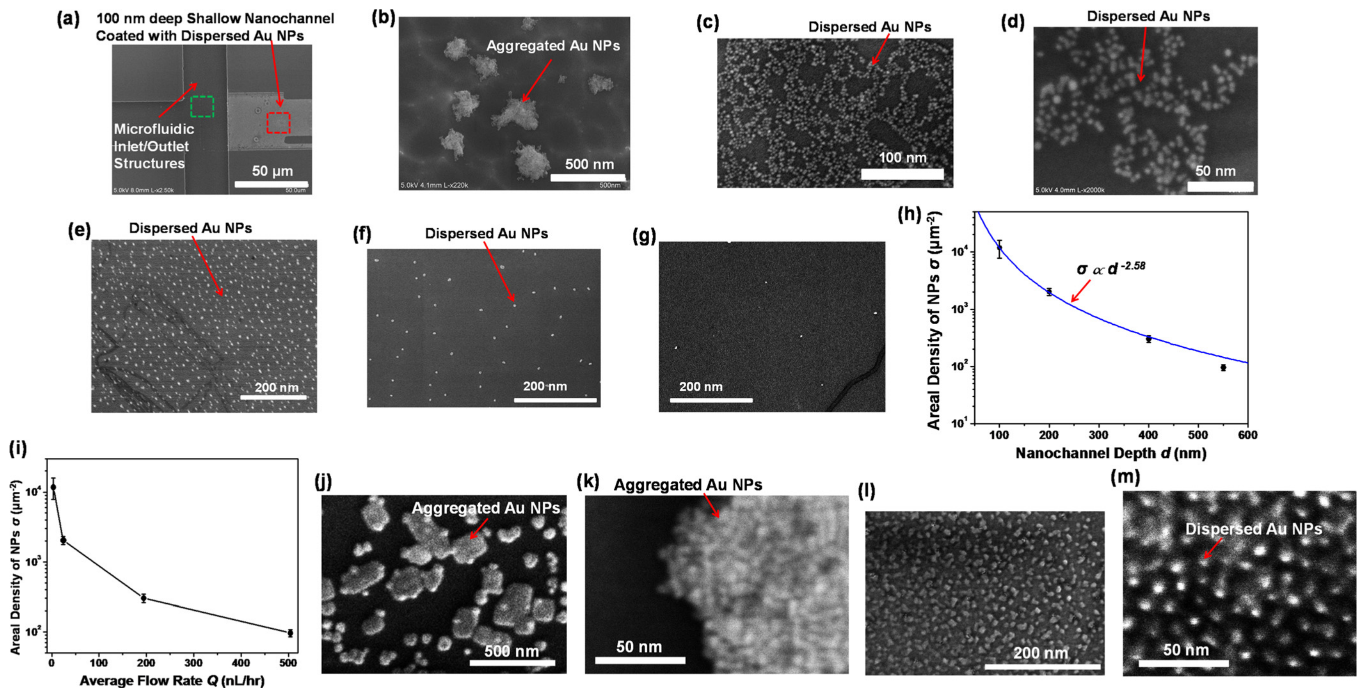

FIG. 2. (Color online) SEM images of Au NPs deposited in sealed shallow nanochannels using NFAA processes: (a) low-magnification SEM image of a shallow nanochannel sensor with 100 nm deep shallow nanochannels and 10 μm deep microfluidic inlet/outlet channels; (b) zoomed SEM image of aggregated Au NPs in microfluidic inlet/outlet channels [i.e., the microfluidic inlet area denoted by the dashed box in (a)]; (c) and (d) zoomed SEM images of well-dispersed Au NPs in the 100 nm deep shallow nanochannels [i.e., the shallow nanochannel area denoted with the dashed box in (a)]; (e), (f), and (g) SEM images of Au NPs deposited in 200, 400, and 550 nm deep shallow nanochannels, respectively; (h) and (i) measured areal densities of NPs plotted as a function of the shallow nanochannel depths and the corresponding average flow rates in the nanochannels. (j) and (k) Low- and high-magnification SEM images, respectively, of 5 nm size Au NPs directly deposited onto a blank SiO_2-coated Si substrate with average areal NP density of $\sim 10^4/\mu m^2$ (surface coverage ratio ~20%). (l) and (m) Low- and high-magnification SEM images, respectively, of the Au NPs deposited in a 200 nm deep shallow nanochannel by using a NFAA process, which also have an areal NP density of $\sim 10^4/\mu m^2$.

average density, the nanoparticles deposited in the shallow nanochannels indeed exhibit a much higher dispersion degree in comparison with the particles deposited in the microfluidic channels. The aggregation degree in a given shallow nanochannel can be reduced by decreasing the average areal density of deposited nanoparticles.

We also performed NFAA in shallow nanochannels with different depths (d) ranging from 100 to 800 nm. For all NFAA processes, the nanofluidic flow duration time is fixed to 6 h. Figures 2(e)–2(g) display the NFAA-deposited Au NPs in 200, 400, and 550 nm deep shallow nanochannels. These results indicate that given a fixed processing time, the areal density of deposited NPs decreases with increasing the shallow nanochannel depth (d). When d is larger than 600 nm, almost no deposition happens (in this case, most injected NPs are only transported from the inlet port to the outlet port with a very low probability of deposition in the shallow nanochannels). Figure 2(h) plots the measured areal densities of NFAA-deposited Au NPs as a function of the shallow nanochannel depths. If the nanofluidic flow in a shallow nanochannel is assumed to be a viscous, quasisteady flow of Newtonian liquid, the volume rate (Q) of the colloidal flow can be approximately evaluated by Eq. (1), where d, W, and L are the depth, width, and length of the shallow nanochannel; μ is the liquid viscosity; and ΔP is the pressure drop between the inlet and the outlet[22]

$$Q = \frac{W\Delta P d^3}{12\mu L}. \tag{1}$$

Assuming that the effective NP concentration (n) remains constant and the probabilities for depositing a NP onto the top and the bottom surfaces are the same, the resultant areal density (σ) of the Au NPs deposited in the shallow nanochannel can be evaluated by Eq. (2), where Δt is the flow duration time, and p is the probability for a NP to be deposited in the shallow nanochannel

$$\sigma = \frac{pnQ\Delta t}{2WL} = p\frac{n\Delta t\Delta P d^3}{24\mu L^2}. \tag{2}$$

Based on Eq. (2), σ is expected to scale with pd^3. If we speculate that p is also dependent on d and scales with d^n, σ is expected to scale with d^{n+3}. As shown in Fig. 2(h), the experimentally measured $\sigma - d$ data can be well fitted with $\sigma \propto d^{-2.58}$, and n is estimated to be -5.58. This analysis indicates that the probability for a NP to be deposited in a shallow nanochannel is strongly dependent on the shallow nanochannel depth, and the reduction of the shallow nanochannel depth can significantly enhance such a probability. To further explore the insights about the effect of the nanochannel depth on the probability for NPs being deposited, we also plot the measured coverage densities of NFAA-deposited NPs as a

function of the calculated average flow rates in the shallow nanochannels with various depths [the calculation is based on Eq. (1)], as shown in Fig. 2(i). Figure 2(i) indicates that given a fixed processing time and pressure drop, the resulted coverage density of NPs in a shallow nanochannel is correlated to the average flow rate in the nanochannel. The lower average flow rate in a shallower nanochannel is expected to result in the longer average time for particles to pass through the nanochannel and therefore the higher probability for particles being deposited in the nanochannel. To further quantitatively understand the kinetic characteristics of the moving and deposited NPs in shallow nanochannels, additional multiphase nanoscale computational fluidic dynamics tools will be developed in the future work.

A question is if applying a nanofluidic flow in a shallow nanochannel can really suppress aggregation of NPs or if this is only due to different processing times and corresponding differences in the final surface coverage densities of NPs. To answer this question, we compared the deposition results obtained using direct deposition and NFAA under a condition, where the final coverage densities of NPs resulted by these two methods are very close and also high enough to enable the evaluation of the effectiveness of NFAA in suppressing aggregation of high-density NPs. Specifically, Figs. 2(j) and 2(k) show the low-magnification and high-magnification SEM images, respectively, of 5 nm size Au NPs directly deposited onto a blank SiO_2-coated Si substrate. Here, directly deposited NPs are specifically defined as the NPs directly deposited onto a blank SiO_2 or Si surface pretreated by using the same process (i.e., RCA cleaning followed with O_2 plasma treatment) as that for treating shallow nanochannels. During this specific direct deposition process, the SiO_2/Si substrate was soaked into an Au NP solution (concentration: 0.05 mg/ml) for 5 min and subsequently dried by using a N_2 gun. As shown in Figs. 2(j) and 2(k), this direct deposition process results in prominent aggregation of NPs, and the resulted surface coverage ratio is ∼20% over the whole sample area (the corresponding average areal density of NPs is

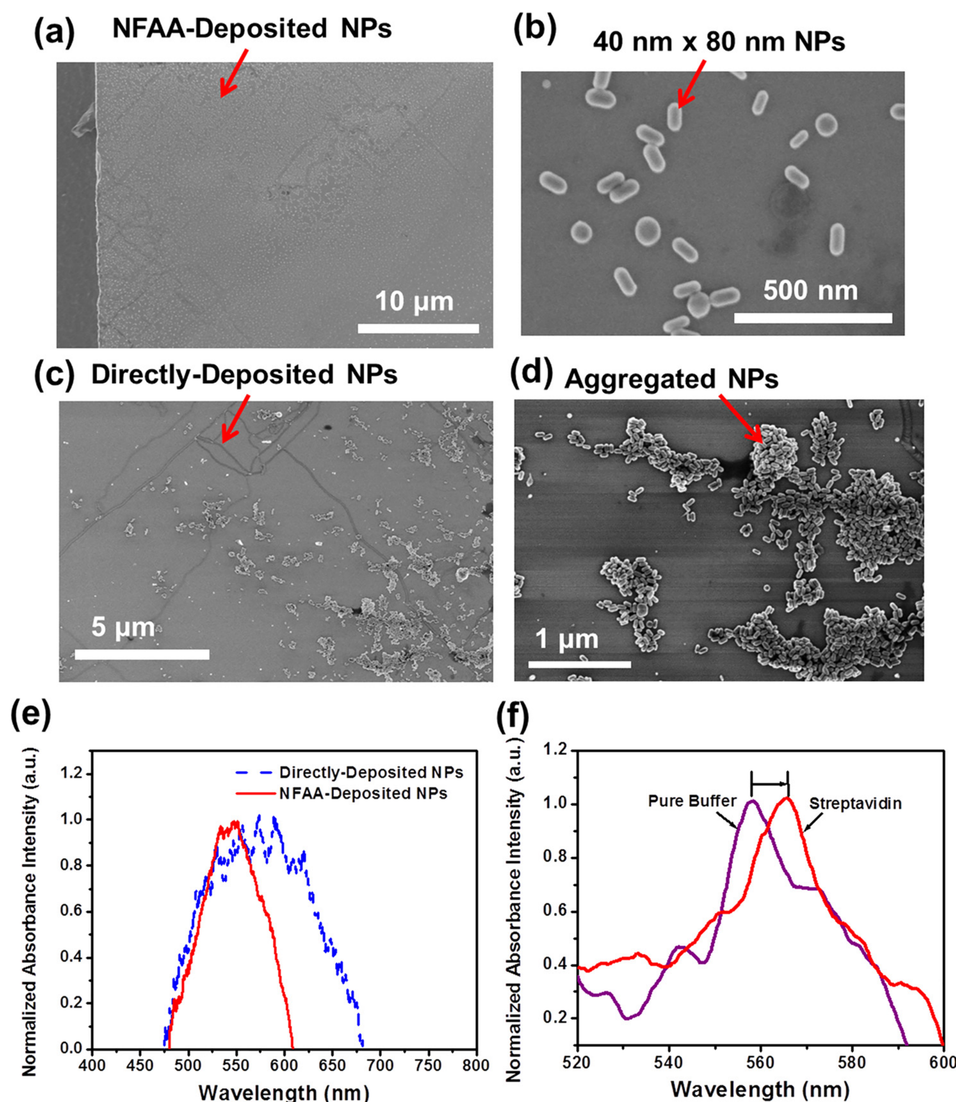

Fig. 3. (Color online) SEM images of (a)/(b) NFAA-deposited and (c)/(d) directly deposited Au NPs; (e) plasmon resonance peaks of NFAA-deposited (solid line) and directly deposited (dashed line) Au NPs; (f) normalized LSPR absorbance spectra measured before and after the presence of 1 ng/ml streptavidin in a shallow nanochannel bearing biotin-functionalized NPs.

estimated to be $\sim 10^4/\mu m^2$). Afterward, we performed a NFAA process to deposit Au NPs in a 200 nm deep shallow nanochannel. Through adjusting the processing time, we can also obtain a NP density of $\sim 10^4/\mu m^2$ (the corresponding processing time is 9 h). Figures 2(l) and 2(m) show the low- and high-magnification SEM images of such Au NPs deposited by the NFAA process, respectively. This result shows that given a fixed areal density of deposited NPs (or surface coverage ratio), the NFAA process can still result in a higher degree of dispersion of deposited NPs in comparison with the direct deposition process without any surface functionalization. It should be noted that the high-magnification SEM images in Figs. 2(k) and 2(m) were captured at the same magnification to obtain a suitable comparison. As shown in Fig. 2(k), although directly deposited NPs can be well resolved under SEM, they preferentially aggregate together, leaving almost no gaps between NPs. However, as shown in Fig. 2(m), NFAA-deposited NPs are well dispersed with relatively uniform nonzero interparticle gaps.

We also measured and compared the light absorbance spectra of NFAA-deposited and directly deposited 40×80 nm size Au NPs from the same colloidal solution. Here, the direct deposition process was also finished through soaking the SiO_2 surface into the Au NP solution (concentration: 0.05 mg/ml) for 5 min and subsequently drying the surface using a N_2 gun. In this measurement, we utilized an optical spectrometer (HR-4000, Ocean optics) to measure the absorbance spectra of deposited Au NPs. In particular, the device under study is illuminated by a tungsten halogen light source (HL-2000 Ocean optics) that can generate visible lights with wavelengths ranging from 400 to 700 nm, and an objective lens is used to focus the excitation light to a small spot ($\sim$0.5 mm size) that can match the entire NP-deposited area on a shallow nanochannel device. The reflected light from the Au NPs is collected by the light probe and transferred into the spectrometer. The final absorbance spectrum of the Au NPs is obtained by subtracting the intensity of the reflected light from the incident light. Figures 3(a) and 3(b) displays the low and high-magnification SEM images of NFAA-deposited Au NPs, respectively, which exhibit a high degree of dispersion. Figures 3(c) and 3(d) show the low and high-magnification SEM images of directly deposited Au NPs on a SiO_2 surface, respectively, which exhibit a significant aggregation of NPs. Figure 3(e) plots the normalized absorbance spectra of the aggregated Au NPs prepared by direct deposition (dashed line) and the well-dispersed Au NPs prepared by NFAA (solid line). Figure 3(e) shows that the absorbance peak of NFAA-deposited NPs exhibits the narrower FWHM in comparison with that of directly deposited Au NPs. This further indicates that NFAA results in the higher degree of dispersion of deposited NPs than direct deposition does. In addition, the absorbance peak of directly deposited NPs exhibits a $\sim$25 nm redshift relative to that of the NFAA-deposited ones. This is also attributed to the aggregation of directly deposited Au NPs, which results in the redshift of the absorbance peak.[23,24] Furthermore, we also preliminarily tested the biosensing performance of NFAA-deposited Au NPs. Specifically, for a biosensing test, 40×80 nm size NFAA-deposited Au NPs in a shallow nanochannel are first functionalized with 10-carboxy-1-decanethiol (C10) dissolved in 50% EtOH, and incubated for 10 h. After the incubation, the shallow nanochannel is briefly rinsed with DI water, and 0.1 mg/ml N-hydroxysuccinimide-biotin in phosphate-buffered saline (PBS) is subsequently incubated on the nanochannel region for 45 min followed by rinsing with DI water. Subsequently, 1 ng/ml streptavidin in PBS is incubated on the shallow nanochannel for 30 min followed by rinsing with DI water. The LSPR absorbance spectra of the Au NPs in the nanochannel are measured at different biodetection

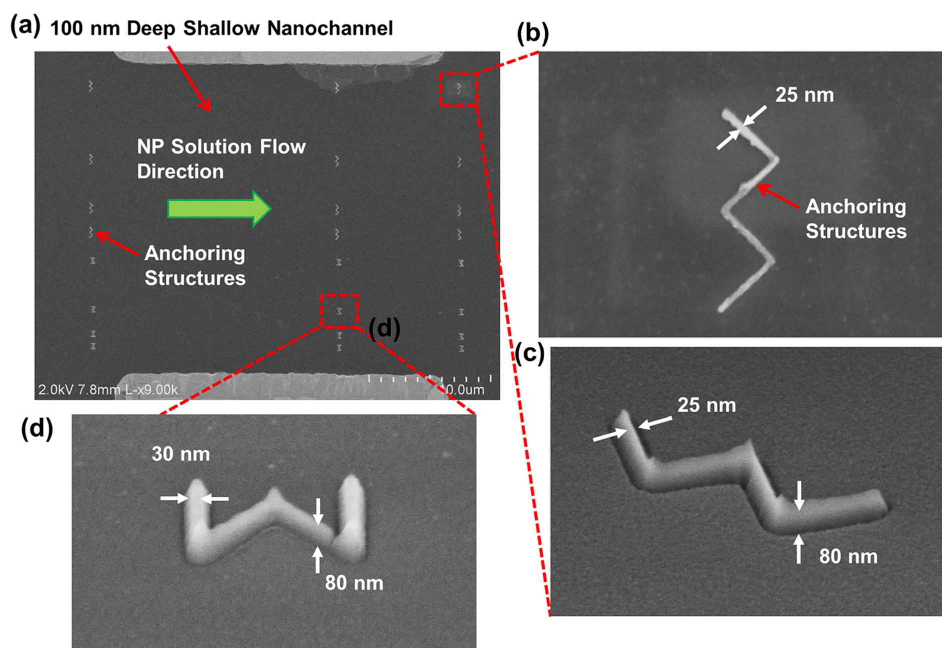

FIG. 4. (Color online) (a) SEM images of the anchoring nanostructures fabricated in a 100 nm deep shallow nanochannel; (b)–(d) The zoomed tilted SEM images of these anchoring nanostructures.

stages. Figure 3(f) shows the normalized LSPR absorbance spectra measured before and after the presence of 1 ng/ml streptavidin in the nanochannel bearing biotin-functionalized NPs. With the presence of 1 ng/ml streptavidin, the LSPR absorbance peak exhibits a redshift of 5 nm relative to that measured under the streptavidin-free condition. This redshift of the absorbance peak is attributed to the refractive index change induced by the streptavidin-biotin binding reaction.[10] This result has preliminarily demonstrated that NFAA-deposited Au NPs can be utilized as a nanoplasmonic biosensor.

Furthermore, to selectively concentrate NPs and other functional nanostructures at specific locations in shallow nanochannels, we used electron-beam lithography (tool: JBX-6300FS, JEOL) and plasma etching to fabricate a set of topographic anchoring nanostructures in the shallow nanochannels. Figure 4 shows the top-view (a) and tilted-view (c) and (d) SEM images of representative Σ- and W-shaped anchoring nanostructures (line width: 25–30 nm, feature height: 80 nm) fabricated in a Si-based shallow nanochannel. The shallow nanochannel devices bearing such anchoring nanostructures were used for performing NFAA processes. For these shallow nanochannel devices, the feature height of anchoring nanostructures is fixed to 80 nm, but the shallow nanochannel depth varies from 100 nm to 1 μm. Other processing conditions for performing NFAA processes are the same as those used for performing NFAA in blank shallow nanochannels. The arrows in Fig. 4(a) indicate the nanofluidic flow direction in the shallow nanochannel. Figure 5(a) shows the SEM image of the 5 nm size Au NPs deposited around a Σ-shaped anchoring nanostructure that is located in a 100 nm deep shallow nanochannel. In such relatively shallow nanochannels, NPs are deposited not only around anchoring nanostructures but also on the flat shallow nanochannel surfaces, but the NP densities around anchoring

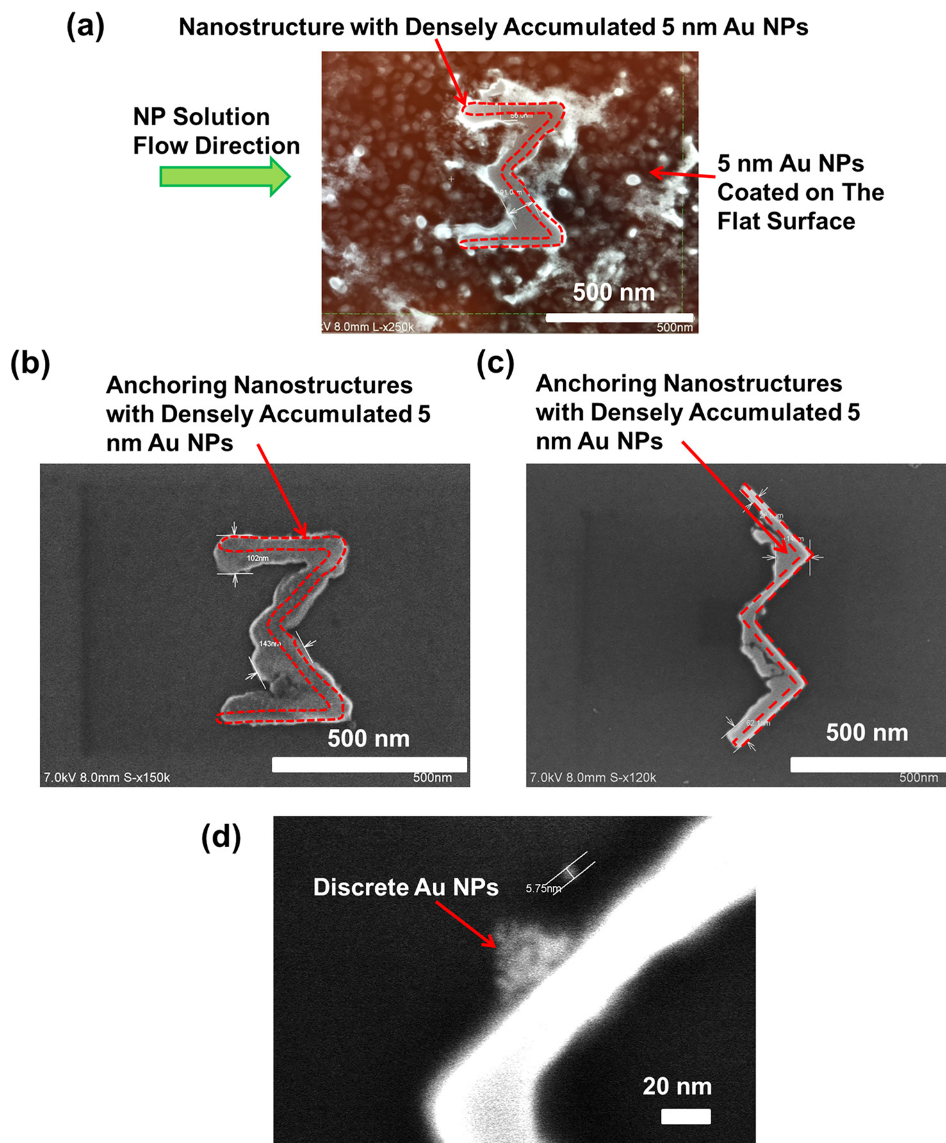

FIG. 5. (Color online) SEM images of the Au NPs deposited around anchoring nanostructures: (a) Au NPs deposited in an 100 nm deep shallow nanochannel with Σ-shaped anchoring nanostructures; (b) and (c) Au NPs deposited in a 800 nm deep shallow nanochannel with Σ-shaped and W-shaped anchoring nanostructures, respectively; and (d) zoomed-in SEM image of Au NPs deposited around an anchoring nanostructure, which was captured by a fast scan and can still exhibit the discreteness of individual Au NPs.

nanostructures are much higher than those on the flat shallow nanochannel surfaces. Figures 5(b) and 5(c) show the SEM images of the Au NPs deposited around a Σ-shaped anchoring nanostructure and a W-shaped one, respectively, which are located in an ~800 nm deep shallow nanochannel. In this case, Au NPs are only accumulated around the anchoring nanostructures, and almost no deposition happens in the blank shallow nanochannel regions. This result is indeed consistent with the NFAA results in blank shallow nanochannel devices with depths >600 nm (see Fig. 2). Using this anchoring-nanostructure-mediated NFAA method, we could realize addressable deposition (or fabrication) of other metallic nanostructures in permanently sealed shallow-nanochannel-based nano/microfluidic devices. Here, it should be noted that the Au NPs shown in Figs. 5(a)–5(c) seem to lose the discreteness and can be hardly resolved under SEM. This is because of (1) the fact that when Au NPs aggregate into bulk structures, they usually lose the discreteness of individual NPs; and (2) that observed under our current SEM system, discrete 5 nm size Au NPs may be quickly melted into continuous nanostructures by the energetic electron beam. Here, it should be pointed out that the discreteness of individual Au NPs is not a critical feature for this work, and Au NPs only serve as a coating material here. For such intentionally accumulated Au NPs (or a material medium), a high degree of dispersion of NPs is indeed not necessary. However, if the NFAA processing time is short enough and the number of Au NPs deposited around an anchoring nanostructure is still small, individual NPs can be still resolved in fast-scanned SEM images. Here, we present one more zoom-in SEM image of Au NPs deposited around an anchoring nanostructure in a short processing time (less than 20 min) [Fig. 5(d)], which was captured by a fast scan and can still exhibit the discreteness of individual Au NPs. Figure 5(d) shows that the material coated on the anchoring nanostructure is indeed made of individual Au NPs.

III. SUMMARY AND CONCLUSIONS

In summary, we present a nanofluidic-flow-assisted-assembly (NFAA) approach for depositing functional nanostructures (e.g., plasmonic NPs) into permanently sealed shallow nanochannel-based nano/microfluidic device structures. In a NFAA process, nanofluidic solution flows carrying functional nanostructures are driven through already fabricated and sealed shallow nanochannels. The large shear rate and stress in such nanofluidic solution flows can result in the deposition of high-areal-density, well-dispersed NPs in shallow nanochannels and effectively prevents the formation of undesirable aggregation of NPs. Using NFAA, we have demonstrated the deposition of well-dispersed 5 nm size Au NPs into shallow nanochannels with various depths (100–600 nm). We found that the resultant areal densities of NPs are strongly dependent on the shallow nanochannel depths and can be tuned in the range of 10^2–10^4 μm^{-2}. The light absorbance peak of NFAA-coated Au NPs exhibits the narrower FWHM than that of the Au NPs directly deposited from the same colloidal solution, further indicating that NFAA can result in the higher degree of dispersion of deposited NPs. Finally, we demonstrated that the additional anchoring nanostructures prestructured in shallow nanochannels, in combination with NFAA processes, can enable addressable deposition of nanoparticles around designated locations. This work provides an approach for depositing plasmonic nanoparticles into permanently sealed shallow nanochannel-based nanofluidic devices. This method could be further generalized and developed to enable introduction of other electrically/optically active nanoscale components into sealed nanofluidic structures and effectively address the incompatibility among the fabrication routes of these different device components.

ACKNOWLEDGMENTS

This work was supported by the University of Michigan (UM)–Shanghai Jiao Tong University (SJTU) Collaborative Research in Applications of Nanotechnology. The authors would like to thank staff of the University of Michigan's Lurie Nanofabrication Facility for providing the support of SEM imaging and device fabrication.

[1]I. Ament, J. Prasad, A. Henkel, S. Schmachtel, and C. Sonnichsen, Nano Lett. **12**, 1092 (2012).
[2]H. Xu, E. J. Bjerneld, M. Kall, and L. Börjesson, Phys. Rev. Lett. **83**, 4357 (1999).
[3]S. K. Ghosh, S. Nath, S. Kundu, K. Esumi, and T. Pal, J. Phys. Chem. B **108**, 13963 (2004).
[4]W. P. Hall, S. N. Ngatia, and R. P. V. Duyne, J. Phys. Chem. C **115**, 1410 (2011).
[5]F. Hao, Y. Sonnefraud, P. V. Dorpe, S. A. Maier, N. J. Halas, and P. Nordlander, Nano Lett. **8**, 3983 (2008).
[6]K. Kneipp, H. Kneipp, V. B. Kartha, R. Manoharan, G. Deinum, I. Itzkan, R. R. Dasari, and M. S. Feld, Phys. Rev. E **57**, 6281 (1998).
[7]K. Kneipp, Y. Wang, H. Kneipp, L. T. Perelman, I. Itzkan, R. R. Dasari, and M. S. Feld, Phys. Rev. Lett. **78**, 1667 (1997).
[8]N. Leopold and B. Lendl, J. Phys. Chem. B **107**, 5723 (2003).
[9]B. Oh, N. Huang, W. Chen, J. H. Seo, P. Chen, T. T. Cornell, T. P. Shanley, J. Fu, and K. Kurabayashi, ACS Nano **8**, 2667 (2014).
[10]B. Sepúlveda, P. C. Angelome, L. M. Lechuga, and L. M. Liz-Marzan, Nano Today **4**, 244 (2009).
[11]C. Huang, K. Bonroy, G. Reekmans, W. Laureyn, K. Verhaegen, I. De Vlaminck, L. Lagae, and G. Borghs, Biomed. Microdevices **11**, 893 (2009).
[12]B. R. Oh, P. Chen, R. Nidetz, W. McHugh, J. Fu, T. P. Shanley, T. T. Cornell, and K. Kurabayashi, ACS Sens. **1**, 941 (2016).
[13]P. Chen, M. T. Chung, W. McHugh, R. Nidetz, Y. Li, J. Fu, T. T. Cornell, T. P. Shanley, and K. Kurabayashi, ACS Nano **9**, 4173 (2015).
[14]K. C. Grabar, P. C. Smith, M. D. Musick, J. A. Davis, D. G. Walter, M. A. Jackson, A. P. Guthrie, and M. J. Natan, J. Am. Chem. Soc. **118**, 1148 (1995).
[15]X. Liang and S. Y. Chou, Nano Lett. **8**, 1472 (2008).
[16]X. Liang, K. J. Morton, R. H. Austin, and S. Y. Chou, Nano Lett. **7**, 3774 (2007).
[17]P. Mao and J. Han, Lab Chip **5**, 837 (2005).
[18]H. Cao, Z. N. Yu, J. Wang, J. O. Tegenfeldt, R. H. Austin, E. Chen, W. Wu, and S. Y. Chou, Appl. Phys. Lett. **81**, 174 (2002).
[19]H. Cao, J. O. Tegenfeldt, R. H. Austin, and S. Y. Chou, Appl. Phys. Lett. **81**, 3058 (2002).
[20]R. H. Austin, J. O. Tegenfeldt, H. Cao, S. Y. Chou, and E. C. Cox, IEEE Trans. Nanotechnol. **1**, 12 (2002).
[21]M. P. Cecchini, V. A. Turek, J. Paget, A. A. Kornyshev, and J. B. Edel, Nat. Mater. **12**, 165 (2013).
[22]M. Dienerowitz, M. Lee, G. Gibson, and M. Padgett, Lab Chip **13**, 2359 (2013).
[23]Z. Liu, H. Wang, H. Li, and X. Wang, Appl. Phys. Lett. **72**, 1823 (1998).
[24]S. J. Oldenburg, R. D. Averitt, S. L. Westcott, and N. J. Halas, Chem. Phys. Lett. **288**, 243 (1998).